

AUSTENITIC BIOMATERIAL CRACKS EVALUATION BY ADVANCED NONDESTRUCTIVE TECHNIQUES

Milan SMETANA¹, Vladimír CHUDACIK¹, Radoslav KONAR², Milos MICIAN²

¹Department of Electromagnetic and Biomedical Engineering, Faculty of Electrical Engineering, University of Zilina, Univerzitna 1, 010 26 Zilina, Slovak Republic

²Department of Technological Engineering, Faculty of Mechanical Engineering, University of Zilina, Univerzitna 1, 010 26 Zilina, Slovak Republic

milan.smetana@fel.uniza.sk, vladimir.chudacik@fel.uniza.sk, radoslav.konar@fstroj.uniza.sk,
milos.mician@fstroj.uniza.sk

DOI: 10.15598/aeec.v15i2.2186

Abstract. *The article deals with Non-Destructive Evaluation (NDE) of austenitic stainless steels. Eddy current, ultrasonic testing and non-contact magnetic field mapping methods are used for this purpose. ECA (Eddy Current Array) and TOFD (Time of Flight Diffraction) are methods that have become widely-used in the field of NDE and this is the reason for their utilization. Magnetic field mapping is nowadays an effective method of evaluation of surface-breaking defects mainly in ferromagnetic materials. The fluxgate sensor-based measurement is presented and discussed. The artificial fatigue and stress-corrosion materials cracks are inspected. Experimental results are presented and discussed in this paper.*

Keywords

Austenitic stainless steels, eddy current testing, fatigue and stress-corrosion material cracks, non-destructive evaluation, time of flight diffraction.

1. Introduction

The role of non-destructive evaluation of material structures is undeniable worldwide. Periodic inspection of components and devices ensures their safe, effective and long-term operation. New methods and devices are still being developed and designed to tackle gradually increasing demands for reliable detection and precise characterization of material discontinuities. Increased R&D activities in the field of Non-Destructive Evaluation (NDE) have been motivated by the need

for precise evaluation of cracks and flaws for the assessment of the expected life of mechanical components. NDE of materials is based on numerous physical principles and phenomena. In recent years, electromagnetic methods, especially Eddy Current Testing (ECT), have attracted increasing attention. Eddy Current Testing (ECT) is one of the widely utilized electromagnetic NDE methods. It works based on the interaction of time-varying electromagnetic field with a conductive body according to the Faraday's electromagnetic induction law. There are many advantages such as high sensitivity for surface breaking defects, high inspection speed, contact-less inspection, versatility, maturity of numerical means that account for continuously enlarging application area of the ECT mainly in nuclear, petrochemical and aviation industries [1], [2] and [5]. Some of the current innovations of the ECT account for increasing information rate of sensed responses and include especially new excitation techniques such as pulsed, chirp and sweep-frequency. Other advances incorporate eddy current sensor arrays, flexible probes and new probes with magnetic sensors such as Hall sensors, Fluxgate magnetometers, SQUID and GMR sensors to detect small perturbation fields. The magnetic field mapping can be performed using the fluxgate sensor non-contactlessly. This allows inspection of the region of interest without external excitation. The gained DC field values, measured in certain positions can provide useful information about the inspected structure [6] and [7].

Ultrasonic Non-Destructive Testing, also known as ultrasonic NDT or simply UT (Ultrasonic Testing), is a method of characterizing the thickness, or internal structure of a test piece through the use of high frequency sound waves. Development in the field leads to new measuring techniques such as TOFD and Phased

Arrays (PA). This measuring technique increased probability of defect identifications because of larger scanning area together with enhancement of the measuring equipment. The problem of defects detection might occur in complex geometry structures where some false echoes can be representing what might lead to incorrect identification of the defects. The frequencies, or pitch, used for UT are many times higher than the limit of human hearing, most commonly in the range from $f = 500$ kHz to $f = 20$ MHz. High frequency sound waves are very directional and they will travel through a medium (e.g. a piece of steel or plastic) until they encounter a boundary of another medium (e.g. air), at which point they reflect back to their source. By analysing these reflections, it is possible to measure the thickness of a test piece, or find evidence of cracks or hidden internal flaws [3], [4] and [8].

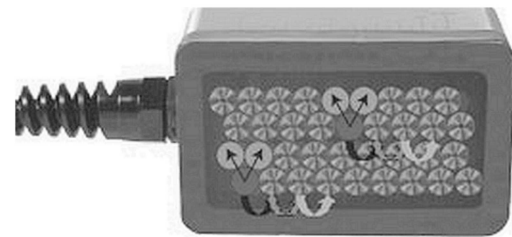
The main aim of this work is to compare three widely-used measuring techniques, applied on the austenitic biomaterials with presence of the real cracks. For this purpose, commercially available equipment is utilized. The reason for such inspection lies in the fact that the inspected material was periodically loaded. Thus, the phase transition (austenitic to the martensitic state) is revealed. Since the transition occurs, magnetic properties are changed and previously non-magnetic material becomes ferromagnetic. Processing and a comparison of measurements is performed. Both the real fatigue and stress-corrosion cracks made under the defined conditions are evaluated.

2. Eddy Current Array Method

Eddy Current Array (ECA) is a nondestructive testing technology that provides the ability to electronically drive multiple eddy current coils, which are placed side by side in the same probe assembly, Fig. 1. Each of the individual eddy current coils of the probe produces a signal relative to the phase and amplitude of the structure below it. This data is referenced to an encoded position and time and represented graphically as a C-scan image. Most conventional eddy current flaw detection techniques can be reproduced with ECA inspections; however, the remarkable advantages of ECA technology allow improved inspection capabilities and significant time savings.

Data acquisition is performed by a multiplex of eddy current coils in a special pattern to avoid mutual inductance between the individual coils. Most conventional eddy current flaw detection techniques can be reproduced with an ECA inspection. With the benefits of single-pass coverage and enhanced imaging capabilities, ECA technology provides a remarkably pow-

erful tool and significant time savings during inspections. The ECA technology includes the following advantages: larger area can be scanned in a single-probe pass, while maintaining a high resolution, less need for complex robotics to move the probe; a simple manual scan is often enough; C-scan imaging improves flaw detection and sizing. Complex shapes can be inspected using probes customized to the profile of the part being inspected [5].



Single coil = raster scan Multiple coils = one-line scan

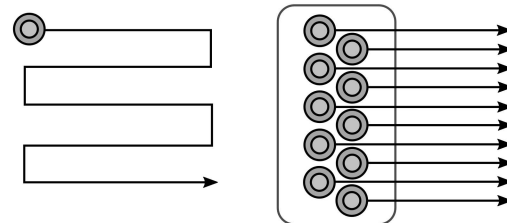


Fig. 1: ECA method: the principle of multiplexing between elements and the scanning principle [5].

3. Time of Flight Diffraction Ultrasonic Technique

The TOFD technique is a newly developed but well established ultrasonic testing technique which has gained popularity in the recent past due to its greater ability in detection, positioning and sizing of the defects. This technique has been widely used in examination of thick wall welds especially in nuclear power plants. The main advantage of this technique is its higher probability of detection and reduced inspection time. In TOFD technique, symmetrical and separate transmitter-receiver pair of ultrasonic probes is maintained at equal distances by a rigid bar. The probes are displaced step wise along a straight line. At each position, an incident ultrasonic wave is emitted with a 45° to 60° angle. The diffracted waves generated after the interaction with the incident wave are converted to an electric pulse that is digitized, and the amplitudes of their samples are converted to grey levels and constitute pixels of one row in the formed image. High amplitudes are displayed as white pixels, low amplitudes as black pixels, and zero amplitude is displayed as grey levels. TOFD

systems use a pair of ultrasonic probes sitting on opposite sides of a welded joint or area of interest. The transmitter probe emits an ultrasonic pulse which is picked up by the receiver probe on the opposite side, Fig. 2. In an undamaged part, the signals picked up by the receiver probe are from two waves, one that travels along the surface (lateral wave) and one that reflects off the far wall (back-wall wave, back-wall reflection). When a discontinuity such as a crack is present, there is a diffraction of the ultrasonic sound wave of the top and bottom tips of the crack. Using the measured time of flight of the pulse, the depth of the crack tips can be calculated automatically by trigonometry application [3] and [4].

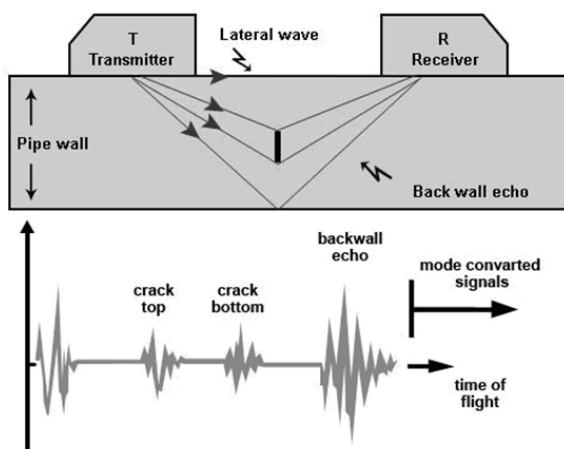


Fig. 2: Principle of the TOFD method, [4].

4. Experimental Set-Up

The configuration for realization of the experiments is introduced to this section.

Real biomaterial fatigue and stress-corrosion cracks are inspected using the ECA, TOFD and magnetic field mapping methods, respectively. The used experimental biomaterial: austenitic stainless steel is inspected in this study. The biomaterial according to the AISI (The American Iron and Steel Institute) standard of grade 316L is evaluated (L = low carbon content), Fig. 3. Conductive plate specimen with thickness of $h = 10$ mm having the electromagnetic parameters of the stainless steel AISI316L is inspected. The material at the initial state (before the initiating of the cracks) had the conductivity of $\sigma = 1.4 \text{ MS}\cdot\text{m}^{-1}$ and the relative permeability of $\mu_r = 1$. After the applied mechanical deformation (loading process) its magnetic properties changed. Thus, the magnetic field mapping procedure could be applied.

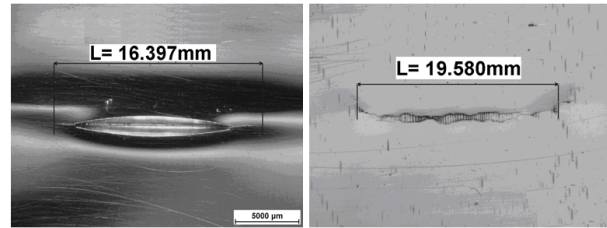


Fig. 3: Microscopy images of the inspected cracks: fatigue crack (left) and stress-corrosion crack (right).

4.1. TOFD Inspection Configuration

The ultrasonic defectoscope OmniScan MX2 (Olympus) is used for the whole measurements. The instrumentation for the TOFD technique consists of these parts: handy scanner Olympus HST-X04, two plexi-glass prisms ST1-60L-IHC (longitudinal ultrasonic wave waveguides), two ultrasonic transducers C563-SM (Tx and Rx configuration), encoder Olympus ENC1-2.5-DE (position measuring) and gel Nord-Test US-A (coupling medium), Fig. 4. Working frequency of the probe $f = 10$ MHz. Encoder resolution $r = 12 \text{ points}\cdot\text{mm}^{-1}$.

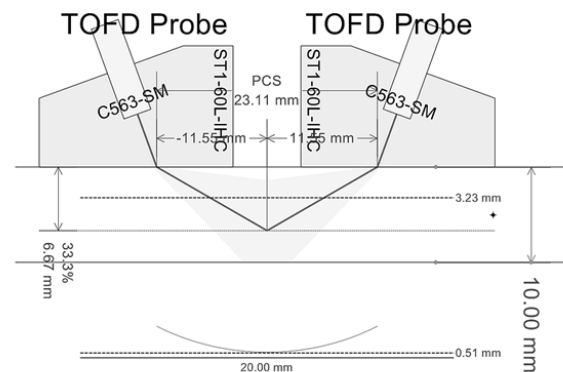


Fig. 4: Spatial configuration during the TOFD inspection.

4.2. ECA Inspection Configuration

The eddy current defectoscope Olympus MX with ECA module is used for the measurements. The ECA probe (SBBR-051-150-032, Olympus) is connected while the harmonic current with the frequency of $f = 150$ kHz is used for an excitation. The specimen is inspected from the near-side.

4.3. Magnetic Field Mapping Inspection

The commercial fluxgate sensor (by Canon Inc.) is used to pick-up the response signal. This sensor is able

to detect a weak magnetic fields, in the frequency range starting from $f = 0$ Hz up to $f = 3.4$ kHz. The scans are performed in axially symmetric direction above the specimens, while the sensor is positioned normally to the surface of the inspected specimen. Measured component of the magnetic field in given direction (sensitive axis) is converted to the output voltage signal: if only ambient external magnetic field is detected, the output signal is equal to approximately $U_{out} = 2.5$ V. Configuration of the sensor is shown in Fig. 5.

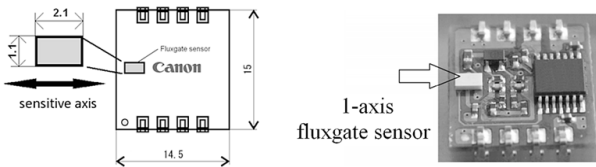


Fig. 5: Spatial configuration of the one-dimensional commercial fluxgate sensor.

The measuring procedure was performed as follows: the fluxgate sensor was used as a Sensing Device (SD), positioned above the material Specimen (S), Fig. 6. For manipulation with the specimen under inspection, we used a Stage Controller (SC) in connection with a three-dimensional linear positioning device (XYZ). The sensed sensor output was acquired by the Data Acquisition device (DAC) with resolution of $res = 16$ bits-channel⁻¹, $f_s = 150$ kS·s⁻¹, filtered with the digital Lock-In amplifier (LI). Personal Computer (PC) in connection with the LabVIEW virtual instrumentation was used for data manipulation and processing.

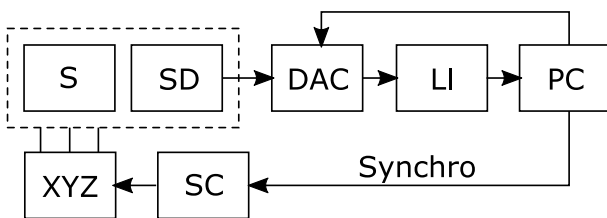


Fig. 6: Configuration of the measuring procedure with the fluxgate sensor.

5. Experimental Results

Results of the experimental measurements are presented in this section.

5.1. Inspection of the Fatigue Crack

Figure 7 displays the results obtained using the ECA technique. Three regions of interest are displayed on the defectoscope's screen: response signal in the Gaussian plane (left corner), time-domain signal analysis

(bottom) and C-scan image (right). Geometry of the crack can be stated using the cursors (threshold lockers) on the screen. As can be seen, measured crack indication has length of $c_L = 15.6$ mm. To extract depth of the crack, the comparative analysis is used and its value is $d_c = 5.05$ mm. Based on these measurements, it can be concluded, that the fatigue crack was clearly identified and its geometry was described. As can be seen from the Fig. 8, the crack indication can be observed via TOFD technique and its geometry can be revealed as follows: crack depth $c_D = 5.5$ mm, crack length of $c_L = 14.8$ mm. Moreover, the real shape of the crack in profile is also visible. However, the length of the the crack cannot be measured very precisely using this method.

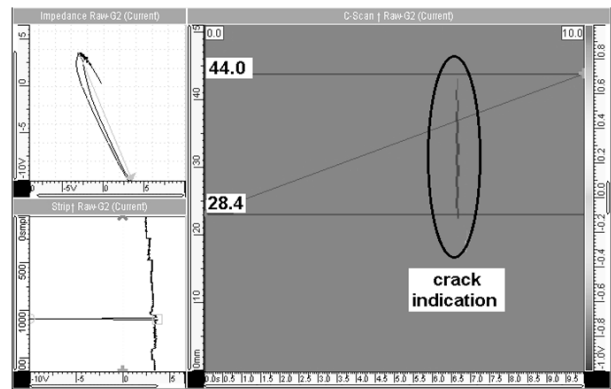


Fig. 7: Fatigue crack inspection using the ECA technique.

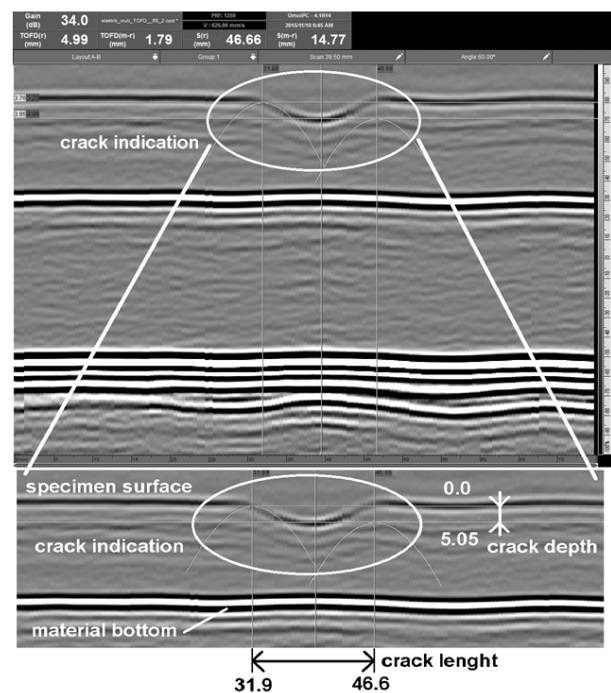


Fig. 8: Fatigue crack inspection using the TOFD technique.

This lies in the fact that curved geometry of the crack is present, as well as the length of the real crack is longer than the artificial notch in the specimen.

Figure 9 shows results of the magnetic field mapping procedure. The normal component (perpendicular to the material's surface) of the magnetic field was sensed and displayed via the fluxgate sensor, while the area of 50 mm × 50 mm was scanned.

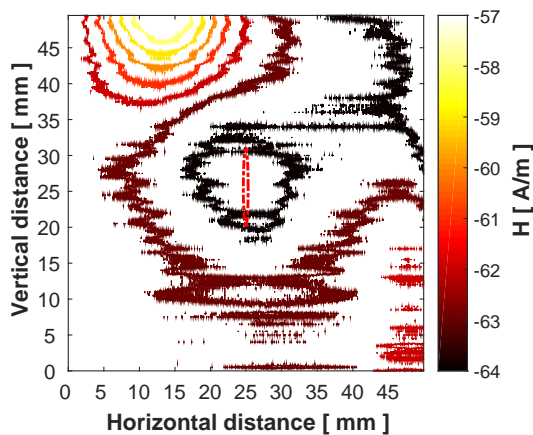


Fig. 9: Intrinsic magnetic field: normal component, fatigue crack.

The contour graph of the magnetic field strength shows its non-homogeneous distribution of the specimen. The real crack borders are shown in the middle of the picture. Further, from the three-dimensional representation of this measurement, Fig. 10, there can be observed change in the direction of the field. This may be interpreted as follows: after the cyclic loading of the austenitic material, this reveals the intrinsic magnetic field. This is caused due to its phase transition. The fatigue crack is located within one of the two poles of the field.

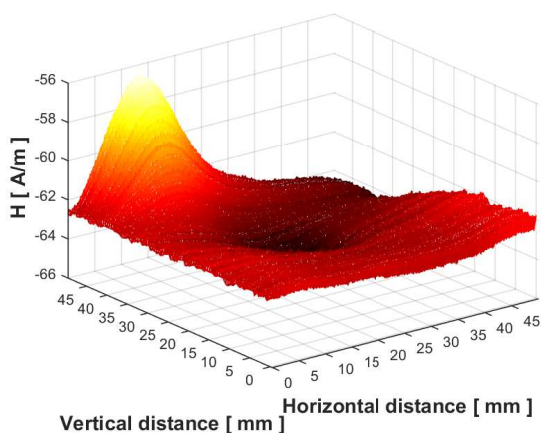


Fig. 10: Fatigue crack: 3D intrinsic magnetic field visualization.

5.2. Inspection of the Stress-Corrosion Crack

Figures 11 and Fig. 12 display results obtained using ECA and TOFD technique, respectively. As can be seen, the crack indication can be observed and its geometry can be revealed as follows: crack depth $c_D = 6.06$ mm, crack length of $c_L = 20.8$ mm (ECA measurement).

Further, the crack dimensions can be described as follows: depth of $c_D = 5.9$ mm, crack length of $c_L = 19.7$ mm (TOFD measurement). In comparison with the FC's results, the shape of this crack is strongly affected by its internal structure.

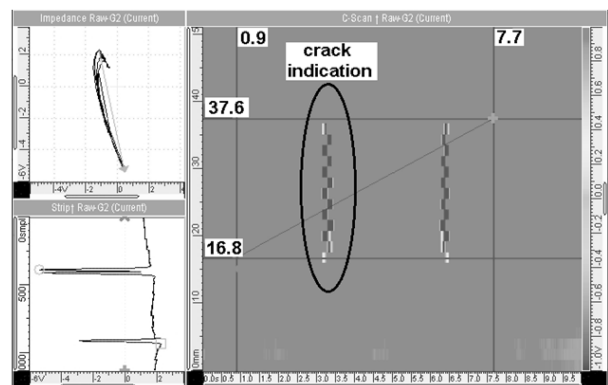


Fig. 11: Stress-corrosion crack inspection using the ECA technique.

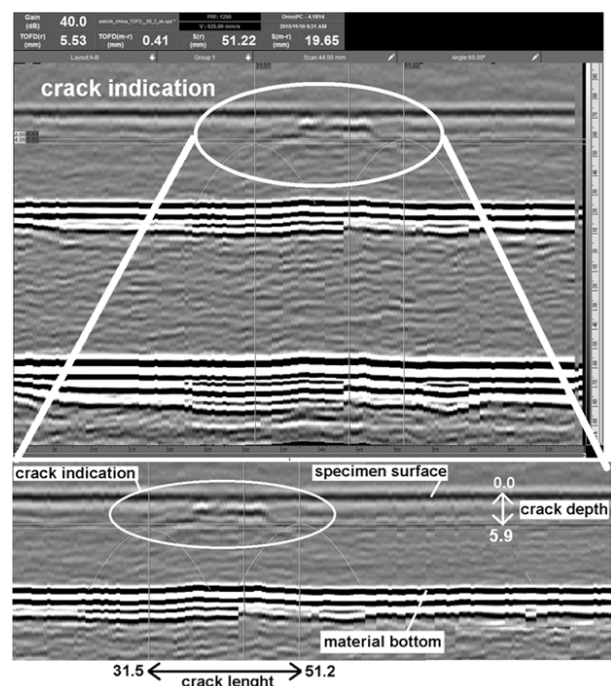


Fig. 12: Stress-corrosion crack inspection using the TOFD technique.

The magnetic field mapping results are displayed in Fig. 13. As can be seen, the presence of the crack cannot be stated from these measurements. Non-homogeneous character of the magnetic field was sensed, however, its distribution has almost no correlation with the crack presence and its position. It can be added that applying static pressure to initiate this crack has no such great effect on creating martensitic domains, in comparison with the periodical loading to produce the fatigue crack. Generally, partially conductive cracks are more difficult to evaluate because of their complex internal structure. To be able to reveal their internal magnetic field in austenitic biomaterials, it is necessary to use more sensitive type of the sensing element (SQUID sensor).

Based on these results it can be concluded that the stress-corrosion crack was identified and its dimensions were in acceptable correlation, measured by the ECA and TOFD methods.

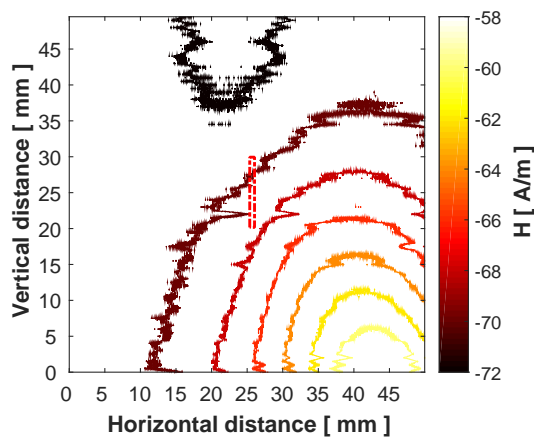


Fig. 13: Intrinsic magnetic field: normal component, SC crack.

6. Conclusion

The article presented a comparison among three advanced procedures of non-destructive evaluation of austenitic biomaterials. The austenitic stainless steel cracks were experimentally inspected using ECA, TOFD and magnetic field mapping technique in this paper. All of these methods represent powerful tools, used in the field of non-destructive evaluation nowadays. According to the results it can be concluded that these methods can identify such types of real cracks. However, due to various physical principles and their specific use, some limitations occurred. Specifically, information about the length of the fatigue crack could not be measured very precisely, using the TOFD method. This is caused by the presence of the specific notch. Moreover, the real fatigue crack length is, in comparison with the TOFD results, longer only about

few tenths of a millimeter. On the other hand, it is more important to reveal the depth of the inspected cracks, non-destructively. This cracks parameter was successfully measured as well. The only way to be the real depths of the cracks stated is to realize measurements destructively. The magnetic field mapping results also brought new useful information about the inspected structure: distribution of the intrinsic field within the specimen may help better understand physical principles which occur during the mechanical (plastic) deformation. On the other hand, presence of the fatigue crack was more dominant in comparison with the stress-corrosion crack by these measurements.

Acknowledgment

The financial support of the project KEGA 034 ZU-4/2015 is gratefully acknowledged.

References

- [1] LI, Y., G. Y. TIAN and A. SIMM. Fast analytical modelling for pulsed eddy current evaluation. *Non-Destructive Testing International*. 2008, vol. 41, iss. 6, pp. 477–483. ISSN 0963-8695. DOI: 10.1016/j.ndteint.2008.02.001.
- [2] GRUGER, H. Array of miniaturized fluxgate sensors for non-destructive testing applications. *Sensors and Actuators A: Physical*. 2003, vol. 106, iss. 1–3, pp. 326–328. ISSN 0924-4247. DOI: 10.1016/S0924-4247(03)00194-8.
- [3] DOPJERA, D., R. KONAR and M. MICIAN. Ultrasonic testing of girth welded joint TOFD and phased array. *Manufacturing Technology*. 2014, vol. 14, no. 3, pp. 281–286. ISSN 1213-2489.
- [4] PATEK, M., R. KONAR, A. SLADEK and N. RADEK. Non-destructive testing of split sleeve welds by the ultrasonic TOFD method. *Manufacturing Technology*. 2014, vol. 14, no. 3, pp. 403–406. ISSN 1213-2489.
- [5] Olympus. *Olympus* [online]. 2017. Available at: <http://www.olympus-ims.com>.
- [6] JANOUSEK, L., M. SMETANA and M. ALMAN. Evaluation of Inductance Coil and Fluxgate Magnetometer under Harmonic and Pulsed Excitations in ECT. *Proceedings of the ISEM 2011 - 15th International Symposium on Applied Electromagnetics and Mechanics*. 2012, vol. 39, no. 1–4, pp. 277–282. ISSN 1383-5416.
- [7] KARBAN, P., F. MACH, P. KUS, D. PANEK and I. DOLEZEL. Numerical solution of coupled

problems using code Agros2D. *Computing*. 2013, vol. 95, iss. 1, pp. 381–408. ISSN 0010-485X.

- [8] KARBAN, P., F. MACH, I. DOLEZEL and J. BARGLIK. Higher-order finite element modeling of rotational induction heating of non-ferromagnetic cylindrical billets. *The International Journal for Computation and Mathematics in Electrical and Electronic Engineering*. 2011, vol. 30, iss. 5, pp. 1517–1527. ISSN 0332-1649.
- [9] VRZGULA, P., M. FATURIK and M. MICIAN. New inspection technologies for identification of failure in the materials and welded joints for area of gas industry. *Manufacturing Technology*. 2014, vol. 14, no. 3, pp. 487–492. ISSN 1213-2489.

About Authors

Milan SMETANA graduated his master study at the Faculty of Electrical Engineering, University of Zilina in 2006. He continued with Ph.D. study in the field of Theory of Electrical Engineering, graduated in 2009. He became an associate professor in the field of Theory of Electrical Engineering in 2014. His research activities are focused mainly on non-destructive evaluation of conductive biomaterials, especially using electromagnetic methods.

Vladimir CHUDACIK graduated his master study in field of Biomedical Engineering at the Department of Electromagnetic and Biomedical

Engineering, Faculty of Electrical Engineering, University of Zilina in 2014. He is nowadays Ph.D. student at the same department in the field of Theory of Electrical Engineering. His research activities are focused on electromagnetic methods of non-destructive evaluation and on implementation of virtual instrumentation in this field.

Radoslav KONAR graduated from the Faculty of Mechanical Engineering, University of Zilina in Zilina, where he received his academic degree Ph.D. in the field of Engineering technology and materials in 2012. It holds several second degree certificates in the field of non-destructive testing in accordance with standard STN EN ISO 9712. From 2012 to the present he works as an assistant professor at the Faculty of Mechanical Engineering, Department of Technological Engineering.

Milos MICIAN graduated from the Faculty of Mechanical Engineering at the University of Zilina. In 2002 he received his Ph.D., study program Engineering Technologies and Materials. In 2007 he earned the title of associate professor. He has been working at the University of Zilina since graduation, first as a Ph.D. student and later as an assistant professor, head of welding and forming department until now, when as a guarantor of several professional subjects devotes himself to lecturing, research activities, management of Ph.D. students and project activities in the field of engineering technology and materials.